Journal of Electroanalytical Chemistry xxx (xxxx) xxx–xxx

Contents lists available at ScienceDirect

Journal of Electroanalytical Chemistry

journal homepage: www.elsevier.com/locate/jelechem

Electrochemical impedance spectroscopy study of the $Li_xMn_2O_4$ interface with natural brine☆

Florencia Marchini, Federico J. Williams, Ernesto J. Calvo*

INQUIMAE, Facultad de Ciencias Exactas y Naturales, Universidad de Buenos Aires, Pabellón 2, Ciudad Universitaria, AR-1428 Buenos Aires, Argentina

ARTICLE INFO

Keywords:
Lithium
Extraction
$LiMn_2O_4$
Impedance
Brine

ABSTRACT

The $LiMn_2O_4$-Polypyrrole electrochemical cell has been shown to extract LiCl from natural brine at low voltage with high selectivity, low energy consumption (5–10 $Wh{\cdot}mol^{-1}$) and good stability. The intercalation/de-intercalation of Li^+ ions in $Li_xMn_2O_4$ ($0 \le x \le 1$) has been studied by electrochemical impedance spectroscopy (EIS) at different potentials and lithium ion concentrations using a modified Randles equivalent electrical circuit for the interface of $Li_xMn_2O_4$ in natural brine from Salar de Olaroz (Jujuy, Argentina). The R_{CT} exhibits two minima at potentials which correspond to $x = 0.25$ and $x = 0.75$ (half filled adsorption sites) respectively and a linear lithium ion concentration dependence of $(Li^+)^{-0.5}$ consistent with a lithium ion transfer adsorption model proposed by Bruce.

1. Introduction

The spinel lithium-manganese mixed oxide $LiMn_2O_4$ is a cathode material in "rocking-chair" rechargeable lithium batteries that intercalates lithium in tetrahedral sites within the octahedral oxygen sublattice in contact with organic solvents containing lithium salts [1,2]. Kanoh has extensively studied the electrochemistry of λ-MnO_2/$LiMn_2O_4$ system in lithium containing aqueous electrolyte [3–8] while La Mantia et al. [9] proposed a LiFePO4 cathode with Ag/AgCl anode and Kim et al. used a λ-MnO_2 cathode with a Ag/AgCl anode [10]; other approaches for lithium recovery have been reviewed elsewhere [11].

An alternative electrochemical method for the extraction of lithium chloride from natural brine or sea water has been developed recently in our research laboratory [11]. Lithium rich brine is processed in an undivided electrochemical reactor comprised of a lithium deficient $Li_xMn_2O_4$ cathode and a chloride reversible polypyrrole (PPy) anode. Under a potential difference of < 1 V, intercalation of lithium ions in the $Li_xMn_2O_4$ electrode and selective capacitive exchange of chloride at the oxidized PPy electrode takes place fast, efficiently, with high selectivity with respect to other ions in the brine, with low energy consumption and has low environmental impact since no water is lost and no chemicals are added.

The effective intercalation and release of Li^+ ions at the interface of $Li_xMn_2O_4$ with natural brine electrolyte and exchange of chloride ions at the polypyrrole modified electrode occurs with high selectivity in the 0.6–1.1 V interval within the $0 < x < 1$ lithium composition range of Li_xMn_2O to λ-MnO_2, and exhibits reproducibility for > 200 cycles of LiCl capture and release [11,12]. Direct evidence of LiCl extraction and release from natural brine has been obtained by ion chromatography of recovery solutions.

XRD patterns have shown that Na^+ is not inserted in the $Li_xMn_2O_4$ crystal structure, but adsorbed sodium and/or occluded brine solutions require a major effort in the rinsing steps to avoid sodium contamination of the LiCl extracted with this method.

The interface of $Li_xMn_2O_4$ with aqueous LiCl electrolyte [4–6] or artificial brine and natural brine [11,12] has been studied to a lesser extent than the same cathode material in contact with non-aqueous electrolyte in lithium ion batteries [14,15] and certainly never in contact with lithium chloride containing natural brine.

In the stable cubic spinel phase $LiMn_2O_4$ lithium ions can be intercalated during discharge from λ-MnO_2 to $LiMn_2O_4$ [14,16]. The mixed oxide, $LiMn_2O_4$ has a spinel structure (space-group Fd3m) and the unit cell contains 56 atoms: A cubic close-packed array of oxygen ions occupying the 32e sites; 16 Mn ions in the octahedral 16d sites (MnO_6) and 8 Li ions in the tetrahedral 8a sites [2].

In the $LiMn_2O_4$ positive lithium ion battery electrode, the available positions for lithium insertion into λ-MnO_2 crystal are tetrahedral 8a sites in the spinel structure [2]. There are two sets of non-equivalent 8a sites which can be occupied in $Li_xMn_2O_4$ (with $x \ll 1$) respectively by

☆ Dedicated to the memory of Professor Roger Parsons who in 1961 as a UNESCO Fellow during his three-month visit initiated the Electrochemistry Group at the University of Buenos Aires, School of Exact and Natural Sciences.

* Corresponding author at: INQUIMAE, Facultad de Ciencias Exactas y Naturales, Universidad de Buenos Aires, Pabellón 2, Ciudad Universitaria, AR-1428 Buenos Aires, Argentina.
E-mail address: calvo@qi.fcen.uba.ar (E.J. Calvo).

https://doi.org/10.1016/j.jelechem.2017.11.071
Received 4 September 2017; Received in revised form 22 November 2017; Accepted 27 November 2017
1572-6657/ © 2017 Elsevier B.V. All rights reserved.

lithium ions each leading to two peaks in the cyclic voltammetry or titration curve. The transition occurs at $Li_{0.5}Mn_2O_4$ composition and the electrode reaction at the $Li_XMn_2O_4$/brine interface during the extraction and release of LiCl from brine is:

$$xLi^+(brine) + Li_{1-x}Mn^{III}_{1-X}Mn^{IV}O_2 + xe^-(cathode) \leftrightharpoons LiMn^{IV}Mn^{III}O_4 \quad (1)$$

Electrochemical impedance spectroscopy has been used to characterize the interface of $LiMn_2O_4$ in contact with non-aqueous electrolyte [15,17–20], and aqueous Li^+ ion electrolyte [4]. The lithium ion phase-transfer reaction at the interface between the lithium manganese oxide electrode and the non-aqueous electrolyte has been studied by impedance spectroscopy by Kobayashi and Uchimoto [21] respectively, and discussed in the framework of Bruce ion adsorption and insertion model [22].

In non-aqueous electrolytes the Nyquist plots in the complex plane exhibit two semicircles in the high and medium frequency ranges and a thin line at a constant angle inclined to the real axis [15,18,21,23].

In the present work we have employed electrochemical impedance spectroscopy to study systematically the effect of electrode potential and lithium ion concentration on the exchange of lithium ions (intercalation and release) at the $Li_XMn_2O_4$ oxide surface in contact with aqueous LiCl solution of different concentration and natural brine from Salar de Olaroz (Provincia de Jujuy, Argentina). The experimental evidence can be rationalized with the two-step lithium ion adsorption model proposed by Peter Bruce with partial de-solvation of an ion in solution adjacent to the intercalation electrode and adsorption of the ion on the electrode surface [22].

2. Experimental

Platinum supported $LiMn_2O_4$ electrode was prepared by thermal decomposition of $LiNO_3/Mn(NO_3)_3$ (Sigma Aldrich) mixed solution (Li/Mn molar ratio = 0.5). A Pt sheet coated with a thin layer of solution containing the cations was initially dried at room temperature, further heated at 650 °C for 12 h and finally cooled at room temperature. Characterization of the thin spinel mixed oxide film was achieved by XRD measurements. The $LiMn_2O_4$ deposit is compact and covers the platinum electrode.

The electrolytes were LiCl (Sigma Aldrich) of several concentrations and natural brine from Salar de Olaroz in the province of Jujuy, Argentina. The natural brine has a chemical composition as revealed by ICP analysis of Na^+ 115.600 ppm (5 M NaCl), K^+ 10.780 ppm (0.28 M KCl), Mg^{2+} 2.618 ppm, Li^+ 975–1280 ppm (0.18 M LiCl), B 1.440 ppm, with a dynamic viscosity of 2.077 Cp, density 1.2710 $g{\cdot}cm^{-3}$ and conductivity 0.1735 $S{\cdot}cm^{-1}$.

The electrochemical lithium extraction to form Pt - λMnO_2 was carried out by applying a constant current density of 15 $\mu A/cm^2$ in a three electrode cell using Ag/AgCl (3 M KCL) as a reference electrode and all potentials herein are quoted with respect to that reference while polypyrrole was the counter electrode.

The chloride reversible polypyrrole counter electrode was obtained by electrochemical polymerization of a 0.1 M pyrrole aqueous solution on large surface area platinum mesh (Goodfellow PT008710) in 1.2 M HCl in water under potential control at 0.8–1 V vs. Ag/AgCl, (3 M KCl, 0.222 V vs. NHE), during 1 h (SI).

Electrochemical potential and current were controlled with an Autolab PGSTAT 30 potentiostat (Autolab, Ecochemie, Holland) with Nova 1.10 software.

Electrochemical impedance spectroscopy (EIS) was measured with an Autolab Potentiostat PGSTAT 30 in a 3-electrode configuration with impedance module FRA-2 under Nova 1.10 software.

The experimental data was fitted to a modified Randles circuit shown in Scheme 1 using *Z*-View® software (Scribner Associated Inc.). In brief, Ro is the uncompensated electrolyte resistance, R_{ct} is the charge transfer resistance due to the ionic exchange of lithium ions at the spinel oxide/brine interface and CPE is a constant phase angle capacitive element due to double layer charging [4]. CPE reflects the frequency dispersion of the impedance components due to the inhomogeneous polycrystalline surface.

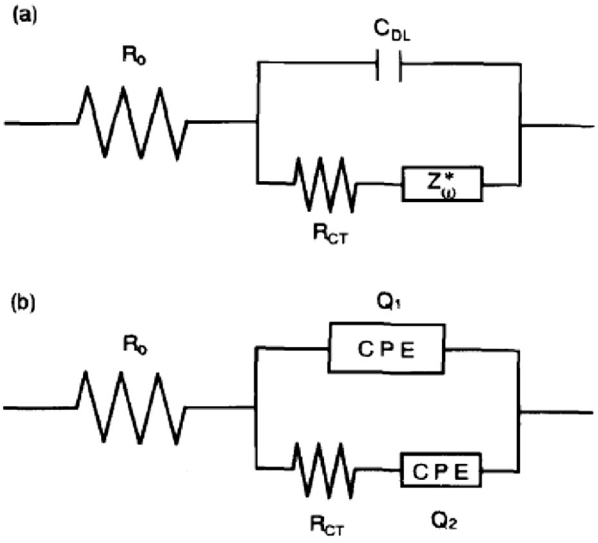

Scheme 1. (a) Randles electrical equivalent circuit for the $LiMn_2O_4$/brine interface and (b) modified Randles equivalent circuit with CPE Q_1 and Q_2 [4].

3. Results and discussion

Fig. 1 shows a cyclic voltammetry curve for $LiMn_2O_4$ at 2 $mV{\cdot}s^{-1}$ during lithium insertion and de-intercalation from natural brine and LiCl respectively. The two pair of peaks correspond to order-disorder phase transition [24] at $Li_{0.5}Mn_2O_4$, which is due to an ordering of lithium on the tetrahedral 8a sites [25].

The peaks are shifted to more positive potentials in the case of brine with respect to pure LiCl of similar concentration due to the high ionic strength and excess of sodium chloride in brine. This results from the high LiCl activity in brine due to strong salting out effect. Also the charge involved in the lithium ion intercalation is less in brine which has been attributed to adsorption of sodium ions at the Li-Mn spinel oxide surface blocking lithium ion adsorption sites as shown by XPS

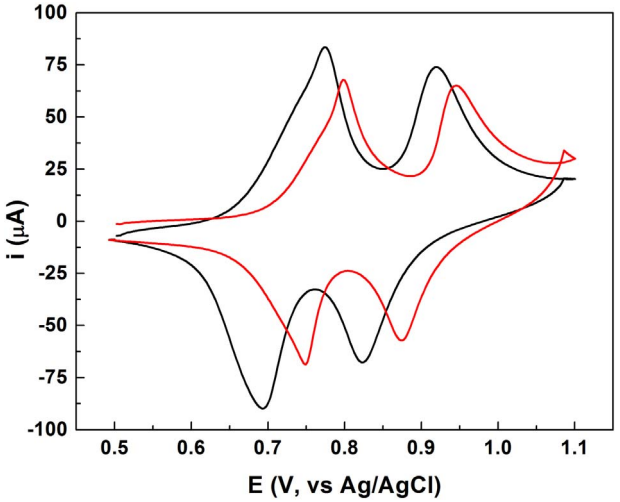

Fig. 1. Cycic voltammetry of $LiMn_2O_4$ in 0.2 M LiCl (black) and natural brine (red) respectively (with 0.2 M LiCl) at 2 $mv{\cdot}s^{-1}$. (For interpretation of the references to color in this figure legend, the reader is referred to the web version of this article.)

[12]. The topotactic lithium extraction from $LixMn_2O_4$ (or insertion into λ-MnO_2) occurs with isotropic shrinkage (or expansion) of the crystal lattice with retention of the original cubic symmetry. Nevertheless, while extracting or inserting Li^+, the crystal structure undergoes several phase transitions between different cubic structures depending on the lithium content. Ohzuku et al. have shown in 1990 structural evidence of two cubic phases for the spinel at different states of charge [26], Further in-situ synchrotron X-ray studies demonstrated that two phase transitions occur between three cubic phases [27]. One phase is present at $x = 1$ while two phases coexist in the range $0.65 < x < 1$. The second phase is unique for $0.55 < x < 0.65$, while a third phase emerges and coexist with the second in the range of $0.27 < x < 0.55$. The third phase at the end of the lithium extraction corresponds to the almost fully de-lithiated structure with only the 12% of the initial lithium. Thus, variation of the Li/Mn ratio exhibits two step electrochemical titration due to insertion in two energetically different surface tetrahedral lithium sites:

$$0.5Li^+ + 2\lambda - MnO_2 + 0.5e^- \rightarrow Li_{0.5}Mn_2O_4 \quad (2)$$

$$0.5Li^+ + Li_{0.5}Mn_2O_4 + 0.5e^- \rightarrow LiMn_2O_4 \quad (3)$$

Fig. 2 shows a chronopotenciometry curve for $LiMn_2O_4$ at 25 mA cm^{-2} during Li^+ insertion and de-intercalation from natural brine.

The two-plateau chronopotetiometry curve corresponds to the two phase transition at $Li_{0.5}Mn_2O_4$ [25]. When homogeneous lithium extraction takes place, there is a change in the free energy of the solid causing the electrode potential to vary. But, when two different phases coexist, the potential is expected to remain constant as the composition changes, giving a flat voltage plateau under galvanostatic conditions, in close agreement to the two plateau observed in the regions of $0.95 < x < 0.63$ and $0.41 < x < 0.19$ for the process:

$$(1-x)Li^+ + Li_xMn_2O_4 + (1-x)e^- \rightarrow LiMn_2O_4 \quad (4)$$

The equilibrium redox potential of the spinel oxide in aqueous lithium ion solutions is given by the Nernstian equation: [3]

$$E = E^0 - \frac{RT}{F} ln\left(\frac{x}{1-x}\right). + \frac{RT}{F} ln\, a_{Li^+} \quad (5)$$

It should be noted that for equilibrium of $LiMn_2O_4$ in LiCl electrolyte the chemical potential of manganese ions is not defined in the electrolyte except for the oxide solubility that defines a concentration of manganese ions in the solution adjacent to the electrode [28].

Fig. 3 depicts typical charging or de-lithiation curves (potential vs. charge) for different lithium chloride concentrations at 25 mA·cm^{-2}

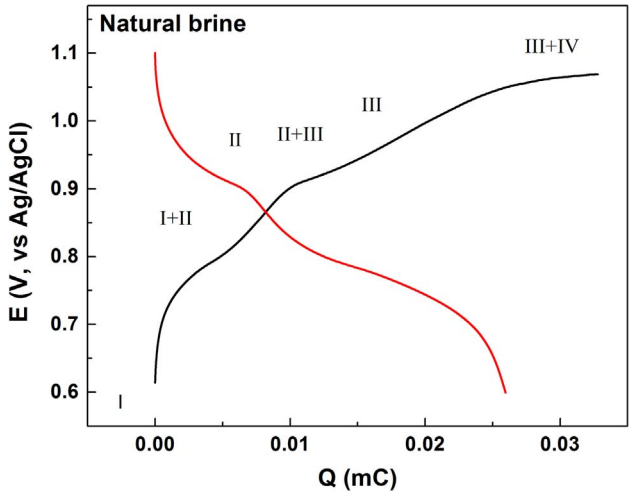

Fig. 2. Lithium chloride extraction and insertion curves at 25 mA·cm^{-2} for $LiMn_2O_4$ in natural brine solution.

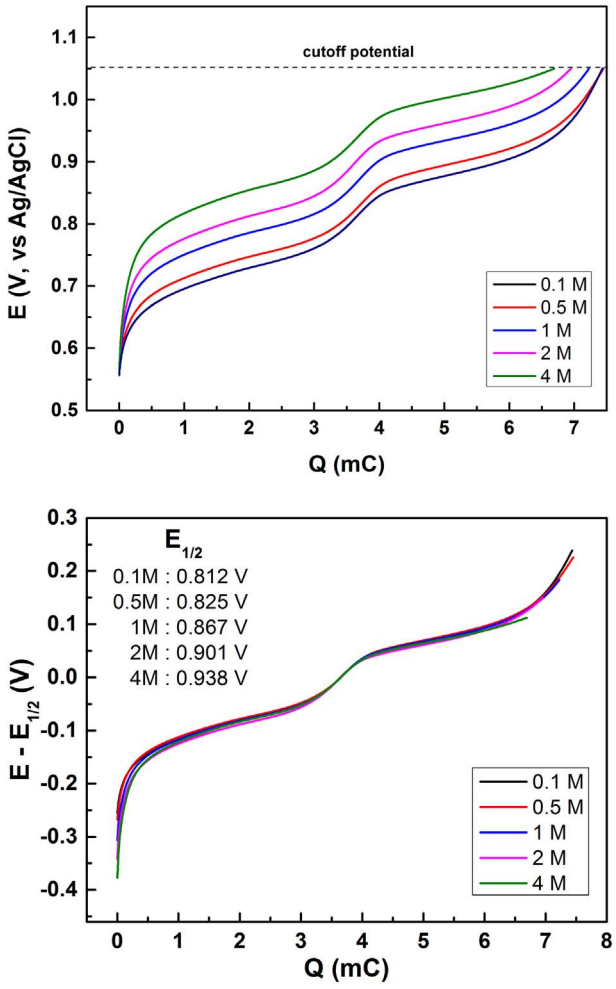

Fig. 3. A: Lithium chloride extraction curves at 25 mA·cm^{-2} at different [LiCl]. B: Extraction curves normalized by subtracting $E_{1/2}$.

which are shifted vertically in potential at increasing lithium chloride concentration as predicted by Eq. (5). A particular constant Li/Mn ratio value is half filled tetrahedral sites in the spinel structure with a nominal stoichiometry, $Li_{0.5}Mn_2O_4$, for which we define $E_{1/2}$. Therefore, if we normalize $(E - E_{1/2})$ and replot, all the curves collapse in one as predicted by Eq. (5). A linear plot of $E_{1/2}$ vs. log a_{Li+} (molal scale) in Supporting Information has a Nernstian behavior with a slope close to 0.059 V.

The thermodynamics of lithium insertion in $Li_xMn_2O_4$ and the voltage profile as a function of x has extensively been described [29]. The shape of the lithiation (insertion) and de-lithiation (extraction) curves at constant current have been described with a lattice gas model [23,30]. The contribution to the chemical potential is proportional to the fraction of occupied lattice sites by the lithium ions (y) and the interaction term, J, is introduced into Eq. (6) to take into account the electrostatic interaction between the lithium ions in the solid.

$$\boldsymbol{E = E^0 - 2.303\frac{RT}{F} log\left(\frac{y}{1-y}\right) + J(x - 0.5)} \quad (6)$$

Notice that Eq. (6) describes the composition of each sub-lattice in the ranges from $0 \le x \le 0.5$ and from $0.5 \le x \le 1$ in $Li_xMn_2O_4$ respectively. There is no way to describe the whole range $0 \le x \le 1$ with a single equation for two interpenetrating cubic sub-lattices [30].

Typical Nyquist complex plane plots for the electrochemical impedance of the LMO/electrolyte interface are shown in Fig. 4 for different LiCl concentrations in aqueous solutions and natural brine respectively. Before measuring the electrochemical impedance, the LMO

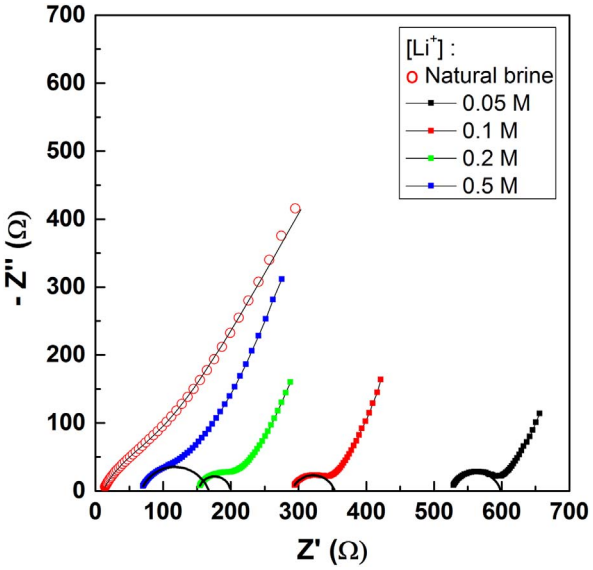

Fig. 4. Complex plane Nyquist plots (5 kHz to 0.1 Hz) for the impedance of $LiMn_2O_4$ in LiCl solutions of different concentration and natural brine at 0.7 V vs Ag/AgCl. E_{ac} = 10 mV. Best fit to the modified Randles equivalent circuit with parameters in Table 1.

electrode was allowed to equilibrate in the respective LiCl aqueous solution. Therefore, the oxide electrode would have a different surface composition (surface state of charge).

The changes of the Nyquist plots at different potentials in 0.2 M and natural brine are shown in Figs. 5 and 6 respectively.

In all cases the impedance data for high frequencies consist of a depressed single semicircle and a diffusional region characterized by constant angle element (CPE). Unlike in non-aqueous solvents, in aqueous solution there is no SEI as confirmed by XPS [12] which is consistent with a single semicircle.

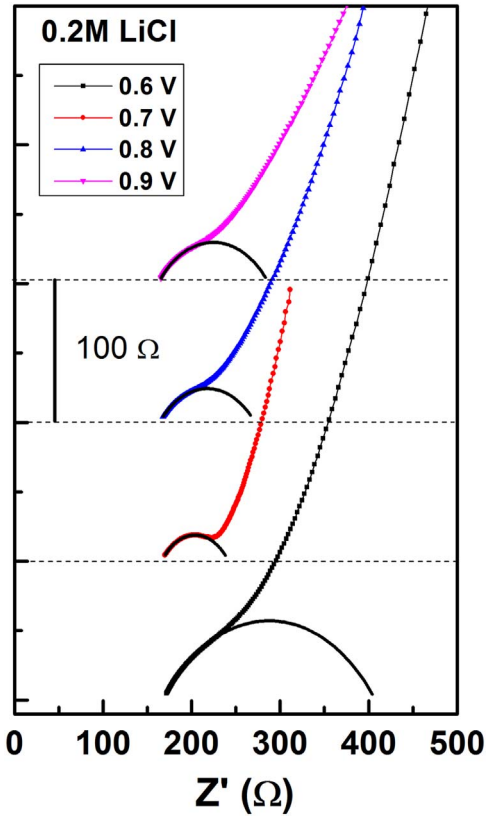

Fig. 5. Complex plane Nyquist plots for the impedance of LMO in 0.2 M LiCl aqueous solutions at different polarization potentials 0.7 V vs Ag/AgCl. E_{ac} = 10 mV. Best fit to the modified Randles equivalent circuit with parameters in Table 1. Curves have been shifted vertically for clarity.

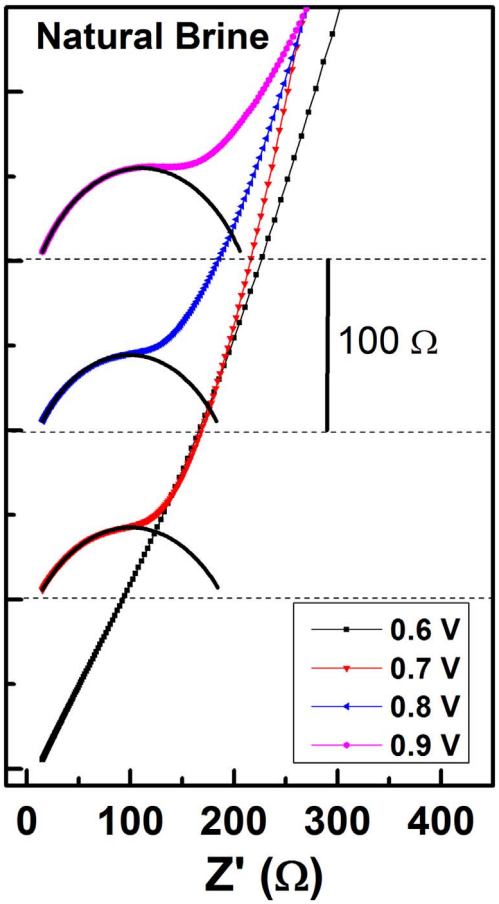

Fig. 6. Complex plane Nyquist plots for the impedance of LMO in natural brine solution at different polarization potentials vs Ag/AgCl. E_{ac} = 10 mV. Circle curves fitted to the modified Randles equivalent electrical circuit. Curves have been shifted vertically for clarity.

Best fit data with the equivalent circuit of Scheme 1, yields circuit elements compiled in Table 1. The CPE index, n, varies between 0.66 and 0.80 which can be attributed to a distribution of time constants for semi-infinite Warburg impedance and finite-length diffusion in the crystal which are not well separated in the complex plane. A typical fit of the semicircles is shown in Figs. 4 and 5 at different concentrations and the electrode potentials for LiCl solutions and Fig. 6 for natural brine.

In aqueous solutions the Nyquist plots exhibit only one semicircle, unlike in aprotic solvents [13,15,19] since there is no formation of SEI as previously reported for LMO in aqueous solutions and verified in our hands by XPS [4,18].

Table 1
Parameters extracted from EIS.

[LiCl] (M)	R_0 (Ohm)	CPE_1 [n] mS	CPE_2 [n] mS	R_{CT}/Ω 0.7 V	R_{CT}/Ω 0.85
0.05	524	60.8 [0.798]	3.58 [0.676]	191	399
0.1	287	73.4 [0.781]	2.37 [0.721]	139	327
0.2	149	109 [0.743]	1.45 [0.699]	106	213
0.5	65.7	167 [0.709]	0.628 [0.712]	90	142
1	36.8	159 [0.732]	0.285 [0.714]	61	116
2	21.8	109 [0.790]	0.136 [0.673]	45	–
Brine	11.2	189 (0.731)	0.429 (0.670)	184	

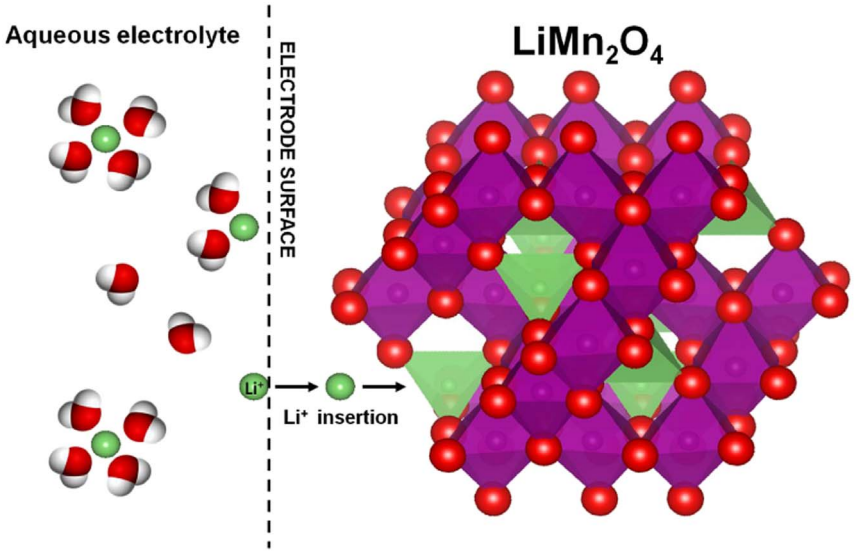

Scheme 2. Schematic process of lithium desolvation, adsorption and insertion into LMO.

The Randles electrical equivalent circuit elements extracted from best fit of the experiment-tal curves are compiled in Table 1. The uncompensated electrolyte resistance values do not depend on electrode potential and decrease with the salt concentration. The charge transfer resistance, Rct, in different LiCl solutions decreases increasing the salt concentration.

3.1. Kinetic model

The process of lithium ion diffusion, de-solvation and adsorption of lithium ions prior to being intercalated into the $Li_xMn_2O_4$ spinel oxide lattice is depicted in Scheme 2. We follow the adsorption model of lithium ion intercalation proposed by Bruce [22] and employed by Kobayashi et al. [21] and Okumura et al. [20] to describe the lithium ion phase transfer at the interface of $Li_xMn_2O_4$ and non-aqueous electrolyte studied by ac-impedance.

As depicted in Scheme 2, this model considers the diffusion of solvated lithium ions towards the spinel oxide surface, the loss of hydration water, adsorption of the ad-ion in a tetrahedral site simultaneous to electron transfer to the Mn^{IV} surface ions and further insertion into the tetrahedral sub lattice of the spinel; lithium-ion diffusion in the crystal and accumulation (consumption) of Li at the electrode, which accompanies phase transition between intercalation stages.

We assume that the velocity of the forward lithiation reaction in the intercalation spinel $Li_{1-X}Mn_2O_4$ electrode is proportional to $\boldsymbol{c_{max}}^{\boldsymbol{surf}}.(1-\theta).\ [\boldsymbol{Li}^+]_{\boldsymbol{soln}}$, where (1-θ) is number of the insertion surface free sites, $\boldsymbol{c_{max}}^{\boldsymbol{surf}}$ the maximum lithium ion concentration at the crytal surface and $[\boldsymbol{Li}^+]_{\boldsymbol{soln}}$ is the lithium ion concentration in the liquid electrolyte near the electrode.

$$\boldsymbol{v_f} = \boldsymbol{k_f}\, \boldsymbol{c_{max}^{surf}}\,(1-\theta)[\boldsymbol{Li}^+]_{\boldsymbol{soln}} \tag{7}$$

Then, the velocity of the backward reaction is proportional to the number of surface sites already occupied by lithium ions, $c_{max.}\theta$:

$$\boldsymbol{v_b} = \boldsymbol{k_b}\boldsymbol{c_{max}^{surf}}\,\theta \tag{8}$$

The current that flows at the $Li_{1\ -\ x}\ Mn_2O_4$ electrode is given by the balance of both intercalation and de-intercalation processes:

$$\boldsymbol{i} = \boldsymbol{nF}\,[\boldsymbol{v_f} - \boldsymbol{v_b}] = \boldsymbol{nF}\ \boldsymbol{c_{max}^{surf}}\,[k_f\,(1-\theta)[Li^+]_{soln} - k_b\theta] \tag{9}$$

With a Butler-Volmer type equation:

$$i = nF\ c_{max}^{surf}\left[k_f^0 e^{-\left(\alpha FE/RT\right)}(1-\theta)[Li^+]_{soln} - k_b^0 e^{-\left((1-\alpha)FE/RT\right)}\theta\right] \tag{10}$$

At equilibrium $i = 0$ and the exchange current density is:

$$i_0 = nFc_{max}^{surf}\,k_0^0\,[Li^+]^{1-\alpha}(1-\theta)^{1-\alpha}\theta^{\alpha} \tag{11}$$

For α = 0.5 the charge transfer resistance due to lithium intercalation is:

$$R_{ct} = \frac{RT}{nFi_0} = \frac{RT}{n^2F^2c_{max}^{surf}\,k_0^0\,[Li^+]^{0.5}(1-\theta)^{0.5}\theta^{0.5}} \tag{12}$$

And the equilibrium potential at i = 0 from Eq. (10):

$$E_{eq} = E^0 + \frac{RT}{F}\,ln\,\frac{(1-\theta)}{\theta} + \frac{RT}{F}\,ln\,[Li^+]_{soln} \tag{13}$$

Notice that in Eq. (13) θ refers to surface sites while in Eq. (6) y describes the lattice sites in the solid.

Therefore Eq. (12) shows that the model predicts that Rct depends on the fraction of available surface lithium ion adsorption sites, (1-θ) and the occupied surface sites, θ both dependent on the electrode potential as described in Eq. (6) and also dependent on the soluble lithium ion concentration.

Fig. 7 shows that R_{ct} depends on the electrode potential with two minima at the half wave potential that corresponds to each half filled surface tetrahedral sites for 0.05 and 0.2 M LiCl solutions respectively and Fig. 8 shows similar plots for natural brine. In Figs. 7 and 8 a comparison with the cyclic voltammetry shows that the minima of R_{ct} coincide with half filled occupancy in each surface site as predicted by Eq. (12).

The linear depependence of R_{ct} with the inverse square root of lithium ion concentration is depicted in Fig. 9 for two selected electrode potentials 0.7 V and 0.85 V in agreement with Eq. (12).

Therefore the electrochemical impedance validates the lithium-ion transfer reaction model at both the $Li_XMn_2O_4$/brine and $Li_XMn_2O_4$/LiCl solution interface.

In previous studies we have demonstrated with XPS spectroscopy that sodium ion, present in large excess with respect to lithium ion in natural brine, adsorbs at the $Li_XMn_2O_4$ surface but does not intercalate into the spinel oxide as proved with XRD [12].

In the present work, we have further studied the effect of sodium ion, present in brine, by electrochemical impedance spectroscopy during the intercalation of lithium ions at the interface of $Li_XMn_2O_4$ with 0.2 M LiCl containing increasing concentration of NaCl and natural brine. Table 2 compiles the impedance parameters. The uncompensated electrolyte solution resistance decreases with increasing the salt concentration and the charge transfer resistance increases with the NaCl concentration.

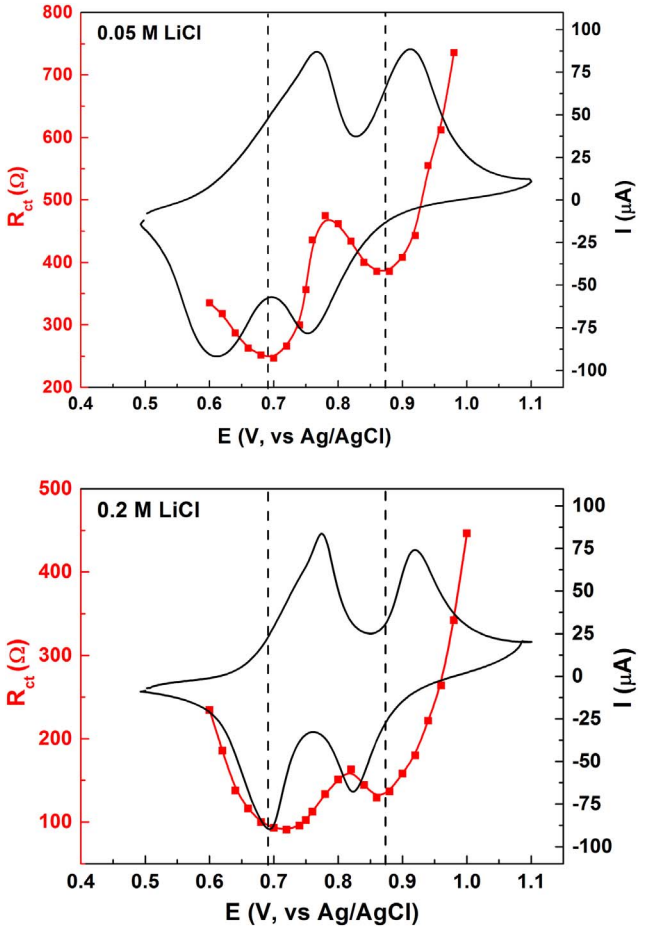

Fig. 7. Plots of R_{ct} vs. electrode potential for 0.05 M (A) and 0.2 M LiCl (B) compared to cyclic voltammetry at 2 mV·s^{-1}.

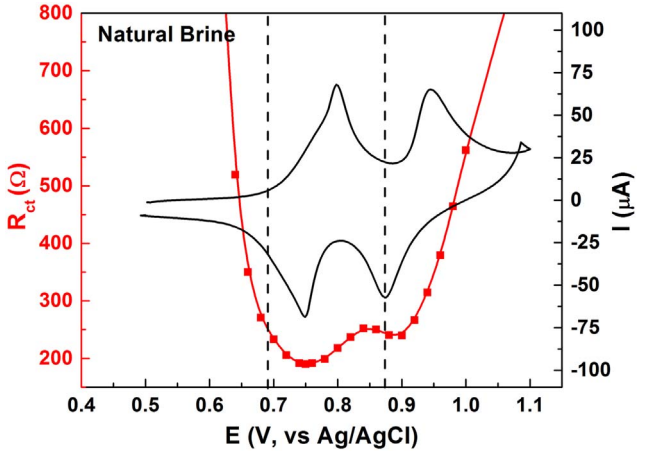

Fig. 8. Plot of R_{ct} vs. electrode potential for natural brine compared to cyclic voltammetry at 2 mV·s^{-1}.

The charge transfer resistance for the insertion of lithium ions into the $Li_XMn_2O_4$ oxide is depicted in Fig. 10 with a clear inhibition effect of NaCl concentration. Interestingly, XPS experiments have shown that if LiCl is replaced by NaCl in the electrolyte the adsorbed sodium ion at the $Li_XMn_2O_4$ surface enables the reduction of surface Mn(IV) to Mn(III) similar to the role of Li^+ even though XRD experiments demonstrate that Na^+ cannot be intercalated in the bulk spinel oxide.

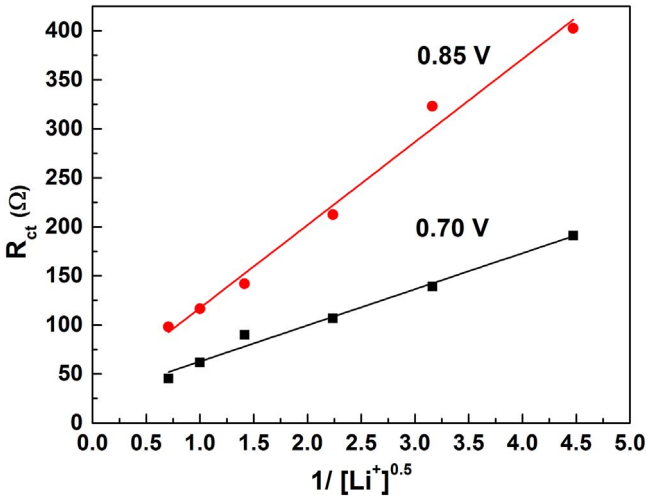

Fig. 9. Plot of Rct vs. $1/[Li]^{0.5}$ at 0.7 V and 0.85 V respectively.

Table 2
Parameters extracted from EIS.

[Li] = 0.2 M, [NaCl] (M)	R_0 (Ohm)	CPE_1 [n] mS	CPE_2 [n] mS	R_{CT}
0.05	116	232 [0.669]	1.49 [0.704]	55.9
0.1	92.3	254 [0.659]	1.35 [0.713]	58.1
0.5	42.9	205 [0.717]	1.38 [0.688]	62.9
1	26.6	250 [0.702]	1.20 [0.692]	64.2
1.8	17.3	229 [0.721]	0.957 [0.687]	75.7
Salmuera	11.2	189 [0.731]	0.429 [0.670]	184

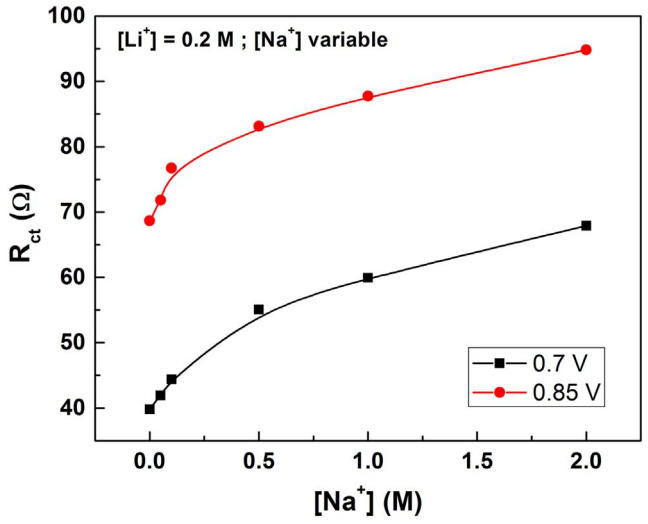

Fig. 10. Plot of R_{ct} vs. $[Na^+]$ in 0.2 M LiCl solution at 0.7 V and 0.85 V.

4. Conclusions

The intercalation/de-intercalation of Li^+ ions in $Li_xMn_2O_4$ ($0 \leq x \leq 1$) has been studied by electrochemical impedance spectroscopy (EIS) at different potential and lithium ion concentration using a modified Randles equivalent electrical circuit for the interface of $Li_xMn_2O_4$ in natural brine from Salar de Olaroz (Jujuy, Argentina). Unlike in non-aqueous solvents, in aqueous solution including natural brine, there is no SEI as confirmed by XPS and only one semicircle can be observed in the complex impedance plot.

The R_{ct} exhibits two minima at potentials which correspond to half-filled tetrahedral sites and a linear lithium ion concentration

dependence of $(Li^+)^{-0.5}$ is consistent with a lithium ion transfer adsorption model proposed by Bruce.

In the presence of sodium added to LiCl solutions and in brine the exchange current density exhibits inhibition due to the adsorption of sodium ions at the oxide/aqueous electrolyte interface but XRD studies have ruled out the insertion of sodium ions into the spinel crystal structure.

Appendix A. Supplementary data

Supplementary data to this article can be found online at https://doi.org/10.1016/j.jelechem.2017.11.071.

References

[1] D. Guyomard, J.M. Tarascon, Li metal-free rechargeable LiMn2O4/carbon cells: their understanding and optimization, J. Electrochem. Soc. 139 (4) (1992) 937–948.
[2] M. Rossouw, A. de Kock, L. de Picciotto, M. Thackeray, W. David, R. Ibberson, Structural aspects of lithium-manganese-oxide electrodes for rechargeable lithium batteries, Mater. Res. Bull. 25 (2) (1990) 173–182.
[3] H. Kanoh, Q. Feng, Y. Miyai, K. Ooi, Equilibrium potentials of spinel-type manganese oxide in aaueous solutions, J. Electrochem. Soc. 140 (11) (1993) 3162–3166.
[4] H. Kanoh, Q. Feng, T. Hirotsu, K. Ooi, AC impedance analysis for Li^+ insertion of a Pt/λ-MnO2 electrode in an aqueous phase, J. Electrochem. Soc. 143 (8) (1996) 2610–2615.
[5] H. Kanoh, K. Ooi, Y. Miyai, S. Katoh, Selective electroinsertion of lithium ions into a Pt/Î-MnO2 electrode in the aqueous phase, Langmuir 7 (9) (1991) 1841–1842.
[6] H. Kanoh, K. Ooi, Y. Miyai, S. Katoh, Electrochemical recovery of lithium ions in the aqueous phase, Sep. Sci. Technol. 28 (1–3) (1993) 643–651.
[7] Q. Feng, Y. Miyai, K. Ooi, H. Kanoh, Kinetic properties of a Pt/lambda-Mn02Electrode for the electroinsertion of lithium ions in an aqueous phase, J. Electrochem. Soc. 142 (3) (1995) 702–707.
[8] H. Kanoh, W. Tang, K. Ooi, In situ raman spectroscopic study on electroinsertion of Li + into a Pt/λ-MnO2 electrode in aqueous solution, Electrochem. Solid-State Lett. 1 (1) (1998) 17–19.
[9] M. Pasta, A. Battistel, F. La Mantia, Batteries for lithium recovery from brines, Energy Environ. Sci. 5 (11) (2012) 9487–9491.
[10] S. Kim, J. Lee, J.S. Kang, K. Jo, S. Kim, Y.E. Sung, J. Yoon, Lithium recovery from brine using a λ-MnO2 activated carbon hybrid supercapacitor system, Chemosphere 125 (2015) 50–56.
[11] L.L. Missoni, F. Marchini, M.D. Pozo, E.J. Calvo, A LiMn2 O4 − Polypyrrole system for the extraction of LiCl from natural brine, J. Electrochem. Soc. 163 (9) (2016) A1898–A1902.
[12] F. Marchini, D. Rubi, M. del Pozo, F.J. Williams, E.J. Calvo, Surface chemistry and lithium-ion exchange in LiMn2O4 for the electrochemical selective extraction of LiCl from natural salt Lake brines, J. Phys. Chem. C 120 (29) (2016) 15875–15883.
[13] F. Marchini, S. Herrera, W. Torres, A.Y. Tesio, F.J. Williams, E.J. Calvo, Surface study of lithium-air battery oxygen cathodes in different solvent-electrolyte pairs, Langmuir 31 (33) (2015) 9236–9245.
[14] J.M. Tarascon, D. Guyomard, Li metal-free rechargeable batteries based on Li1 + xMn2O4 cathodes (0 â‰¤ x â‰¤ 1) and carbon anodes, J. Electrochem. Soc. 138 (10) (1991) 2864–2868.
[15] K.A. Striebel, E. Sakai, E.J. Cairns, Impedance studies of the thin film LiMn2O4/electrolyte interface, J. Electrochem. Soc. 149 (1) (2002).
[16] D. Guyomard, J.M. Tarascon, Rechargeable Li1 + xMn2O4carbon cells with a new electrolyte composition, J. Electrochem. Soc. 140 (11) (1993) 3071–3081.
[17] Quan-Chao Zhuang, Xiang-Yun Qiu, Shou-Dong Xu, Ying-Huai Qiang, S.-G. Sun, Diagnosis of electrochemical impedance spectroscopy in lithium ion batteries, in: I. Belharouak (Ed.), Lithium Ion Batteries. New Developments, InTech, Rijeka, Croatia, 2012.
[18] I. Yamada, T. Abe, Y. Iriyama, Z. Ogumi, Lithium-ion transfer at LiMn2O4 thin film electrode prepared by pulsed laser deposition, Electrochem. Commun. 5 (6) (2003) 502–505.
[19] Q.C. Zhuang, T. Wei, L.L. Du, Y.L. Cui, L. Fang, S.G. Sun, An electrochemical impedance spectroscopic study of the electronic and ionic transport properties of spinel LiMn2O4, J. Phys. Chem. C 114 (18) (2010) 8614–8621.
[20] T. Okumura, T. Fukutsuka, K. Matsumoto, Y. Orikasa, H. Arai, Z. Ogumi, Y. Uchimoto, Lithium-ion transfer reaction at the interface between partially fluorinated insertion electrodes and electrolyte solutions, J. Phys. Chem. C 115 (26) (2011) 12990–12994.
[21] S. Kobayashi, Y. Uchimoto, Lithium ion phase-transfer reaction at the interface between the lithium manganese oxide electrode and the nonaqueous electrolyte, J. Phys. Chem. B 109 (27) (2005) 13322–13326.
[22] P.G. Bruce, M.Y. Saidi, The mechanism of electrointercalation, J. Electroanal. Chem. 322 (1–2) (1992) 93–105.
[23] S.W. Kim, S.I. Pyun, Analysis of cell impedance measured on the LiMn2O4 film electrode by PITT and EIS with Monte Carlo simulation, J. Electroanal. Chem. 528 (1–2) (2002) 114–120.
[24] Y. Gao, J.N. Reimers, J.R. Dahn, Changes in the voltage profile of Li/Li1-xMn2-xO4 cells as a function of x, Phys. Rev. B: Condens. Matter Mater. Phys. 54 (6) (1996) 3878–3883.
[25] D. Guyomard, J.M. Tarascon, Rocking-chair or lithium-ion rechargeable lithium batteries, Adv. Mater. 6 (5) (1994) 408–412.
[26] T. Ohzuku, M. Kitagawa, T. Hirai, Electrochemistry of manganese dioxide in lithium nonaqueous cell: III. X-ray diffractional study on the reduction of spinel-related manganese dioxide, J. Electrochem. Soc. 137 (3) (1990) 769–775.
[27] X.Q. Yang, X. Sun, S.J. Lee, J. McBreen, S. Mukerjee, M.L. Daroux, X.K. Xing, In situ synchrotron X-ray diffraction studies of the phase transitions in LixMn2O4 cathode materials, Electrochem. Solid-State Lett. 2 (2–4) (1999) 157–160.
[28] K.E. Heusler, Oxide electrodes, Electrochim. Acta 28 (4) (1983) 439–449.
[29] S.W. Kim, S. Lee, S. Pyun, The fundamentals and advancedsof solid-state electrocemistry intercalation (insertion) and deintercalation (extractioon) in solid state electrodes, in: V.V. Kharton (Ed.), Solid Electrochemistry I. Fundamentals, Materials and their Applications, WILEY-VCH Verlag GmbH & Co. KGaA, Weinheim, Germany, 2011.
[30] S.I. Pyun, S.W. Kim, Thermodynamic approach to electrochemical lithium intercalation into Li1-δMn2O4 electrode prepared by sol-gel method, Mol. Cryst. Liq. Cryst. Sci. Technol., Sect. A 341 (2000) 155–162.